

# Spherical Message Passing for 3D Graph Networks

Yi Liu\*<sup>1</sup> Limei Wang\*<sup>1</sup> Meng Liu<sup>1</sup> Xuan Zhang<sup>1</sup> Bora Oztekin<sup>1</sup> Shuiwang Ji<sup>1</sup>

## Abstract

We consider representation learning from 3D graphs in which each node is associated with a spatial position in 3D. This is an under explored area of research, and a principled framework is currently lacking. In this work, we propose a generic framework, known as the 3D graph network (3DGN), to provide a unified interface at different levels of granularity for 3D graphs. Built on 3DGN, we propose the spherical message passing (SMP) as a novel and specific scheme for realizing the 3DGN framework in the spherical coordinate system (SCS). We conduct formal analyses and show that the relative location of each node in 3D graphs is uniquely defined in the SMP scheme. Thus, our SMP represents a complete and accurate architecture for learning from 3D graphs in the SCS. We derive physically-based representations of geometric information and propose the SphereNet for learning representations of 3D graphs. We show that existing 3D deep models can be viewed as special cases of the SphereNet. Experimental results demonstrate that the use of complete and accurate 3D information in 3DGN and SphereNet leads to significant performance improvements in prediction tasks.

## 1. Introduction

In many real-world studies, structured objects such as molecules and proteins are naturally modeled as graphs (Gori et al., 2005; Wu et al., 2018; Shervashidze et al., 2011; Fout et al., 2017; Liu et al., 2020; Wang et al., 2020). With the advances of deep learning, graph neural networks (GNNs) have been developed for learning from graph data (Kipf & Welling, 2017; Veličković et al., 2018; Xu et al., 2019; Gao & Ji, 2019; Gao et al., 2020; Yuan & Ji, 2020). In Battaglia et al. (2018), existing GNN methods have been unified to the general graph network (GN)

framework and can be realized by message passing architectures (Gilmer et al., 2017; Sanchez-Gonzalez et al., 2020). The original GN framework is developed for regular graphs rather than 3D graphs. Generally, a 3D graph contains 3D coordinates for each node given in the Cartesian system along with the graph structure (Liu et al., 2019; Townshend et al., 2019; Axelrod & Gomez-Bombarelli, 2020). Different types of relative 3D information can be derived from 3D graphs, and they can be important in some applications, such as bond lengths and angles in molecular modeling.

In this work, we propose the 3D graph network (3DGN) as a generic framework for 3D graphs. The 3DGN aims at providing a clear interface at different levels of graph granularity such that researchers can easily develop novel methods for 3D graphs. We note that the original Cartesian coordinates in 3D graphs usually cannot serve as direct inputs to computational models, as they contain severely redundant information that may hurt model performance. In addition, they are not invariant to translation and rotation of input graphs. Hence, following message passing neural networks (MPNNs) (Scarselli et al., 2008; Gilmer et al., 2017; Vignac et al., 2020), we further propose a novel message passing scheme, known as the spherical message passing (SMP), for realizing the 3DGN framework. Based on formal analysis in the spherical coordinate system (SCS), we show that the relative location of each node in 3D graphs is uniquely determined in the SMP scheme. Hence, our SMP represents a complete and accurate architecture for realizing the 3DGN in SCS. As the encoded 3D information is the relative positional information such as distances between pairwise nodes, SMP yields predictions that are invariant to translation and rotation of input graphs.

We apply the SMP to real-world problems, where meaningful physical representations are important. By integrating the SMP and physical representations approximating the density functional theory, we develop the spherical message passing neural networks, known as the SphereNet, for 3D graph learning. We show that existing models for 3D graphs, such as SchNet (Schütt et al., 2017) and DimeNet (Klicpera et al., 2020b), are special cases of our SphereNet, as they only encode partial 3D information. We conduct experiments on various types of datasets including QM9, OC20, and MD17. Experimental results show that compared with baseline methods, SphereNet achieves the best performance

\*Equal contribution <sup>1</sup>Department of Computer Science & Engineering, Texas A&M University, TX, USA. Correspondence to: Shuiwang Ji <sji@tamu.edu>.

without increasing computations. Ablation study reveals contributions of different 3D information, and demonstrates the advances of the proposed SMP.

## 2. Related Work

### 2.1. Graph Neural Networks

Graph neural networks (GNNs) are an emerging area of research. Notable GNN methods include GCN (Kipf & Welling, 2017; Defferrard et al., 2016), GAT (Veličković et al., 2018), GraphSAGE (Hamilton et al., 2017), GIN (Xu et al., 2019), LGCN (Gao et al., 2018), GG-NN (Li et al., 2016), DGCNN (Zhang et al., 2018), graph U-Nets (Gao & Ji, 2019), etc. Currently, message passing neural networks (MPNNs) (Gilmer et al., 2017) are viewed as the most general architectures for realizing GNNs. These networks and architectures are further extended and unified to a more generic framework, known as the graph network (GN) in Battaglia et al. (2018). The key steps for the GN framework include information aggregation and information update across different levels of granularity, such as nodes, edges, or the whole graph. However, the GN framework does not incorporate the 3D positional information when performing the aggregation and update processes, while such information is vital in some real-world applications.

### 2.2. Methods for 3D Graphs

Formally, 3D graphs refer to graphs in which 3D positions for all nodes are given in the Cartesian system and are useful in deriving graph representations. Generally, original Cartesian coordinates in 3D graphs can not serve as direct inputs to computational models. Otherwise, they may hurt model performance and the generated predictions would not be invariant to translation and rotation of input graphs. Hence, several types of relative 3D information can be derived based on absolute Cartesian coordinates, such as distances between nodes, angles between edges, angles between planes, etc. Such 3D information is invariant to translation and rotation and is important in some applications. For instance, in molecular modeling, the 3D molecular information includes bond lengths, angles between bonds, and bond rotations. These information plays a crucial role in molecular representation learning.

The development of methods for 3D graphs is in early stage, and existing studies focus on leveraging different types of 3D information. The SchNet (Schütt et al., 2017) incorporates the distance information during the information aggregation stage by using continuous-filter convolutional layers. The PhysNet (Unke & Meuwly, 2019) integrates both the node features and distance information in the proposed interaction block. The DimeNet (Klicpera et al., 2020b) is developed based on the PhysNet and moves a step forward

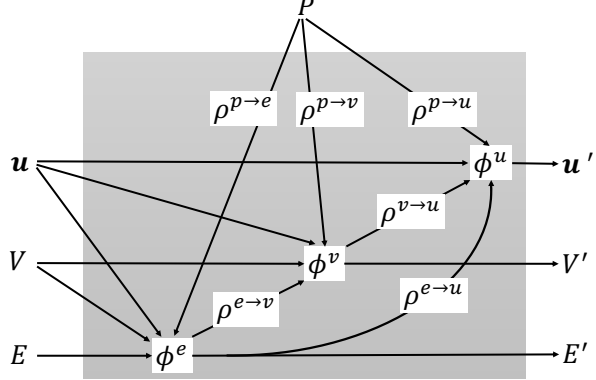


Figure 1. An illustration of the computational steps for our proposed 3DGN framework.

by considering both distance and angle information in the interaction block. In addition to the above methods that explicitly integrate 3D information during the information aggregation process, the OrbNet (Qiao et al., 2020) combines distance information with the atomic orbital theory to design important SAAO features as inputs to GNNs. Generally, the use of 3D positional information usually results in improved performance. However, there lacks a unified and rigorous framework to systematically incorporate 3D information in the message passing schemes.

## 3. A Generic Framework for 3D Graphs

In machine learning, structured objects can be naturally represented as graphs. For instance, molecular representation learning is a key task in many fields, including biophysics and material science (Xie & Grossman, 2018; Wu et al., 2018). When modeling molecules as graphs, atoms are represented as nodes, and bonds between atoms are modeled as edges. In addition, characteristics of atoms and bonds, e.g., atom and bond types, can be encoded as node and edge attributes. With the advances of deep learning, GNNs have been developed to learn features from input graphs. There exist numerous architectures for GNNs, and Battaglia et al. (2018) unify and extend these architectures by proposing the graph network (GN) framework. The GN framework in Battaglia et al. (2018) is based on graphs without 3D positional information of the input graphs. In some applications, such as molecular property prediction, the 3D information, such as bond lengths, angles between bonds, bond rotations, is of great importance for making accurate predictions. To this end, we propose the 3D graph network (3DGN) as a new and generic framework to explicitly consider 3D positional information in real-world data. Our 3DGN is a general framework that provides a clear interface for manipulating structured objects represented as 3D graphs.

A 3D graph is represented as a 4-tuple  $G = (u, V, E, P)$ . The  $u \in \mathbb{R}^{d_u}$  is a global feature vector for the graph

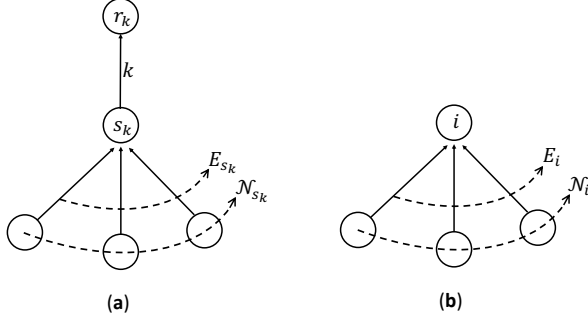


Figure 2. Illustrations of the functions  $\phi^e$  (a) and  $\phi^v$  (b).

$G$ .  $V = \{\mathbf{v}_i\}_{i=1:n}$  is the set of node features, where each  $\mathbf{v}_i \in \mathbb{R}^{d_v}$  is the feature vector for the node  $i$ .  $E = \{(\mathbf{e}_k, r_k, s_k)\}_{k=1:m}$  is the set of edges, where each  $\mathbf{e}_k \in \mathbb{R}^{d_e}$  is the feature vector,  $r_k$  is the index of the receiver node, and  $s_k$  is the index of the sender node for the edge  $k$ .  $P = \{\mathbf{r}_h\}_{h=1:n}$  is the set of 3D Cartesian coordinates that contains 3D spatial information for each node. In addition, we let  $E_i = \{(\mathbf{e}_k, r_k, s_k)\}_{r_k=i, k=1:m}$  denote the set of edges that point to the node  $i$ , and  $\mathcal{N}_i$  denote the indices of incoming nodes of node  $i$ .

The computational steps of our proposed 3DGN framework are illustrated in Fig. 1. The used functions include a set of  $\phi$  functions and a set of  $\rho$  functions. Generally, the  $\phi$  functions are applied to nodes, edges, or the whole graph as information update functions for the corresponding geometries, while the  $\rho$  functions are used to aggregate information from one type of geometry to another. The outputs include the updated global feature vector  $\mathbf{u}' \in \mathbb{R}^{d_u}$ , the updated node features  $V' = \{\mathbf{v}'_i\}_{i=1:n}$ , and the updated edges  $E' = \{(\mathbf{e}'_k, r_k, s_k)\}_{k=1:m}$ . Formally, our proposed 3DGN framework is defined as

$$\begin{aligned} \mathbf{e}'_k &= \phi^e \left( \mathbf{e}_k, \mathbf{v}_{r_k}, \mathbf{v}_{s_k}, E_{s_k}, \mathbf{u}, \rho^{p \rightarrow e} \left( \{\mathbf{r}_h\}_{h=r_k \cup s_k \cup \mathcal{N}_{s_k}} \right) \right), \\ \mathbf{v}'_i &= \phi^v \left( \mathbf{v}_i, \rho^{e \rightarrow v} (E_i), \mathbf{u}, \rho^{p \rightarrow v} \left( \{\mathbf{r}_h\}_{h=i \cup \mathcal{N}_i} \right) \right), \\ \mathbf{u}' &= \phi^u \left( \rho^{e \rightarrow u} (E'), \rho^{v \rightarrow u} (V'), \mathbf{u}, \rho^{p \rightarrow u} \left( \{\mathbf{r}_h\}_{h=1:n} \right) \right). \end{aligned} \quad (1)$$

Specifically, the function  $\phi^e$  is applied to each edge  $k$  and outputs the updated edge vector  $\mathbf{e}'_k$ . The indices of the input geometries to  $\phi^e$  are illustrated in Fig. 2 (a). Correspondingly, the inputs include the old edge vector  $\mathbf{e}_k$ , the receiver node vector  $\mathbf{v}_{r_k}$ , the sender node vector  $\mathbf{v}_{s_k}$ , the set of edges  $E_{s_k}$  that point to the node  $s_k$ , and the 3D positional information for all the nodes connected by the edge  $k$  and edges in  $E_{s_k}$  with the index set as  $r_k \cup s_k \cup \mathcal{N}_{s_k}$ . The function  $\rho^{p \rightarrow e}$  aggregates 3D information from these nodes to update the edge  $k$ . The function  $\phi^v$  is used for per-node update and generates the new node vector  $\mathbf{v}'_i$  for each node  $i$ . An illustration of the indices of the inputs to  $\phi^v$  is provided in Fig. 2 (b). The inputs include the old node vector  $\mathbf{v}_i$ , the set of edges  $E_i$  that point to the node  $i$ , and 3D information for all the related nodes (the index set is  $i \cup \mathcal{N}_i$ ). The

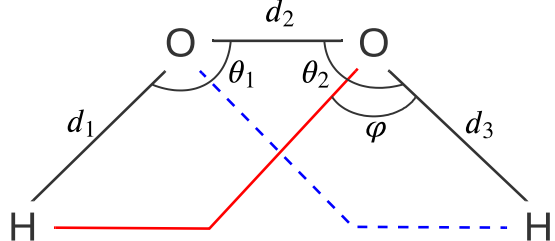


Figure 3. The chemical structure of the  $\text{H}_2\text{O}_2$ .

functions  $\rho^{e \rightarrow v}$  and  $\rho^{p \rightarrow v}$  are applied to aggregate the input edge features and the input nodes' positional information for updating the node  $i$ , respectively. The function  $\phi^u$  is used to update the global graph feature, while the functions  $\rho^{e \rightarrow u}$ ,  $\rho^{v \rightarrow u}$ , and  $\rho^{p \rightarrow u}$  aggregate information from all the edge features, all the node features, and 3D information for all the nodes, respectively.

Importantly, we explicitly incorporate positional information contained in  $P$ , and use three aggregation functions  $\rho^{p \rightarrow e}$ ,  $\rho^{p \rightarrow v}$ , and  $\rho^{p \rightarrow u}$  to compute positional representations for different geometries. Note that absolute Cartesian coordinates stored in  $P$  are not invariant to translation and rotation, and usually contain excessive useless information. Hence, they are not used as immediate inputs to machine learning models. The  $\rho$  functions can be flexibly adapted to generate relative 3D information that is invariant to translation and rotation. For example, when updating node features in Eq. (1),  $\rho^{p \rightarrow v}$  can be adapted to a radial basis function (RBF) that computes distances between node  $i$  and each of its incoming edges in  $E_i$ .

## 4. Spherical Message Passing Neural Networks

Currently, the class of message passing neural networks (MPNNs) (Gilmer et al., 2017) are the most widely used architectures for GNNs. In this work, we aim at constructing a suitable and specific message passing scheme that incorporates 3D positional information, thus realizing the 3DGN framework described in Sec. 3. Importantly, the encoded 3D information should be relative positional information that is invariant to translation and rotation of real-world graphs like molecules. To this end, we propose to perform message passing in the spherical coordinate system (SCS), resulting in a novel scheme known as spherical message passing (SMP). Based on our formal analysis in the SCS, we argue and show that our SMP represents a complete and accurate architecture for realizing 3DGN in SCS. By integrating the SMP and physically based representations, we propose the spherical message passing neural networks, known as the SphereNet, for learning representations for 3D graph data. We show that existing 3DGN architectures, such as SchNet and DimeNet, are special cases of our SphereNet, as they

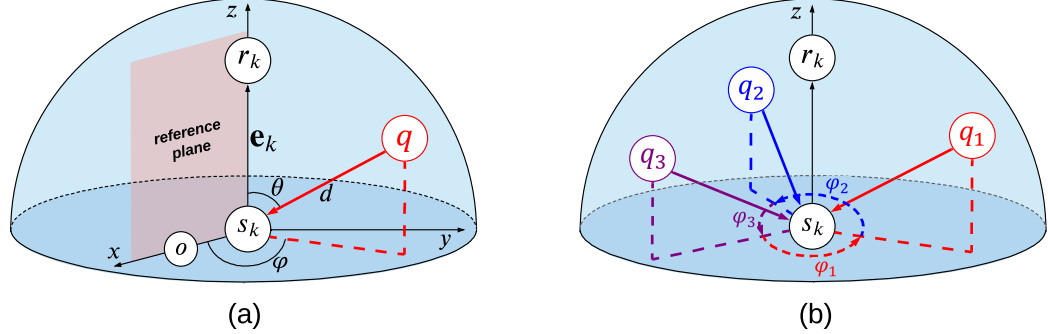


Figure 4. (a). The message aggregation scheme for the spherical message passing. (b). An illustration for computing torsion angles in the spherical message passing architecture.

capture partial 3D information.

#### 4.1. Spherical Message Passing

We first investigate the structure identification of 3D graphs in the spherical coordinate system. For any point in the SCS, its location is specified by a 3-tuple  $(d, \theta, \varphi)$ , where  $d$ ,  $\theta$ , and  $\varphi$  denote the radial distance, polar angle, and the azimuthal angle, respectively. When modeling 3D graphs in the SCS, any node  $i$  can be the origin of a local SCS, and  $d$ ,  $\theta$ , and  $\varphi$  naturally become the edge length, the angle between edges, and the torsion angle, respectively. Thus, the relative location of each neighboring node of node  $i$  can be specified by the corresponding tuple  $(d, \theta, \varphi)$ . Similarly, the relative location of each node in the 3D graph can be determined, leading to the identified graph structure, which is naturally invariant to translation and rotation of the input graph. The SCS can be easily converted from the Cartesian coordinate system, where the 3D positional information  $P$ , introduced in Sec. 3, is defined. Thus, the tuple  $(d, \theta, \varphi)$  can be easily obtained from  $P$ .

We use a molecular graph as an example to show how  $d$ ,  $\theta$ , and  $\varphi$  are vital for the graph structure identification. The chemical structure of the hydrogen peroxide ( $\text{H}_2\text{O}_2$ ) is shown in Fig. 3. It is obvious that the structure is uniquely defined by the three bond lengths  $d_1$ ,  $d_2$ ,  $d_3$ , the two bond angles  $\theta_1$ ,  $\theta_2$ , and the torsion angle  $\varphi$ . Note that the two O-H bonds can rotate around the O-O bond without changing any of the bond lengths and bond angles. In this situation, however, the torsion angle  $\varphi$  changes and the structure of the  $\text{H}_2\text{O}_2$  varies accordingly. Hence, the torsion angle is necessary for determining structures of molecular graphs. The importance of torsion angle has also been demonstrated in related research domains. [Garg et al. \(2020\)](#) formally show that the torsion angle along with the port numbering can improve the expressive power of GNNs in distinguishing geometric graph properties, such as girth and circumference, etc. Other studies ([Ingraham et al., 2019](#); [Simm et al., 2020](#)) reveal that protein sequences and molecules can be accurately generated by considering the torsion angle in the

given 3D structures. In this work, we propose SMP to systematically consider distance, angle, and torsion information for completely determining structures of 3D graphs.

An illustration of the message aggregation scheme for SMP is provided in Fig. 4 (a). Based on Eq. (1), the embedding of the node  $r_k$  is obtained by aggregating each incoming message  $e_k$ . The message  $e_k$  is updated based on  $E_{s_k}$ , the set of incoming edges pointing to the node  $s_k$ . Let  $q$  denote the sender node of any edge in  $E_{s_k}$ . Hence, we can define a local SCS, where  $s_k$  serves as the origin, and the direction of the message  $e_k$  naturally serves as the  $z$ -axis. We define a neighboring node  $o$  of  $s_k$  as the reference node. Thus, the reference plane is formed by three nodes  $s_k$ ,  $r_k$ , and  $o$ . For node  $q$ , its location is uniquely defined by the tuple  $(d, \theta, \varphi)$ , as shown in Fig. 4 (a). Specifically,  $d$  determines its distance to the node  $s_k$ ,  $\theta$  specifies its direction to update the message  $e_k$ . Apparently, the relative location of the node  $q$  is not completely determined when fixing  $d$  and  $\theta$  only. For instance,  $q$  can rotate around  $s_k$  without changing  $d$  and  $\theta$ . To determine the location of  $q$  completely, we propose to use the torsion angle  $\varphi$ , which is formed by the defined reference plane and the plane spanned by  $s_k$ ,  $r_k$ , and  $q$ . Intuitively, as an advanced message passing architecture in spherical coordinates for 3DGN, SMP can determine the relative location for any neighboring node  $q$  by considering all the distance, angle, and torsion information, leading to more informative and accurate 3D representations.

Generally, the node  $s_k$  may have several neighboring nodes, which we denote as  $q_1, \dots, q_t$ . It is easy to compute the corresponding bond lengths and bond angles for these  $t$  nodes. The SMP computes torsion angles by projecting all the  $t$  nodes to the plane that is perpendicular to  $e_k$  and intersect with  $s_k$ . Then on this plane, the torsion angles are formed in a predefined direction, such as the anticlockwise direction. By doing this, any node naturally becomes the reference node for its next node in the anticlockwise direction. Notably, the sum of these  $t$  torsion angles is  $2\pi$ . A simplified case is illustrated in Fig. 4 (b). The node  $s_k$  has three neighboring nodes  $q_1$ ,  $q_2$ , and  $q_3$ ;  $q_1$  is the reference node for  $q_1$ ,

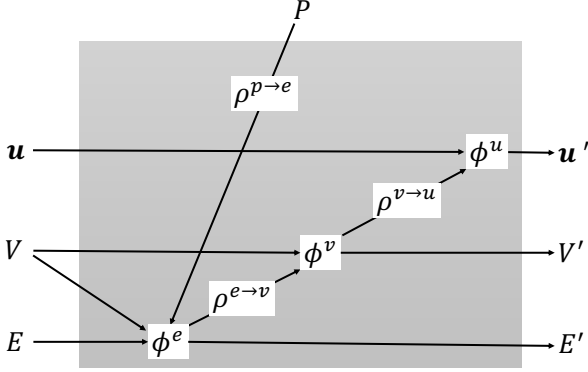


Figure 5. An illustration of the computational steps for the sphere message passing.

and they form  $\varphi_1$ ;  $q_1$  is the reference node for  $q_2$ , and they form  $\varphi_2$ ; similarly,  $q_2$  is the reference node for  $q_3$ , and they form  $\varphi_3$ . It is obvious that the sum of  $\varphi_1$ ,  $\varphi_2$ , and  $\varphi_3$  is  $2\pi$ .

Our 3DGN is a general framework considering the 3D positional information. The unified framework makes it easier for researchers to develop novel architectures on 3D graphs for real-world applications. In this work, we move a step forward by proposing the spherical message passing as a specific and novel architecture for the 3DGN. Formally, the definition of the SMP can be obtained by realizing Eq. (1) in the SCS as

$$\begin{aligned} \mathbf{e}'_k &= \phi^e \left( \mathbf{e}_k, \mathbf{v}_{r_k}, \mathbf{v}_{s_k}, E_{s_k}, \rho^{p \rightarrow e} \left( \{\mathbf{r}_h\}_{h=r_k \cup s_k \cup \mathcal{N}_{s_k}} \right) \right), \\ \mathbf{v}'_i &= \phi^v \left( \mathbf{v}_i, \rho^{e \rightarrow v} (E_i) \right), \\ \mathbf{u}' &= \phi^u \left( \mathbf{u}, \rho^{v \rightarrow u} (V') \right). \end{aligned} \quad (2)$$

The 3D information in  $P$  is converted and used to update each edge feature  $\mathbf{e}^k$ . Hence, for the three positional aggregation functions  $\rho^{p \rightarrow e}$ ,  $\rho^{p \rightarrow v}$ , and  $\rho^{p \rightarrow u}$ , SMP only uses  $\rho^{p \rightarrow e}$  for edge updates. The functions  $\phi^e$ ,  $\phi^v$ , and  $\phi^u$  can be implemented in different ways, such as using neural networks and mathematical operations. The computational flow of SMP can be obtained by removing several connections in Fig. 1 and is given in Fig. 5. We propose to implement the function  $\rho^{p \rightarrow e}$  as the physically based representation  $\Psi(d, \theta, \varphi)$ , which is the solution to the Schrödinger equation approximating the density functional theory (DFT).

#### 4.2. Physical Solutions Approximating DFT

The obtained 3-tuple  $(d, \theta, \varphi)$  determines the relative location of any node in the graph. However, in some applications, such as molecular representation learning, the 3-tuple  $(d, \theta, \varphi)$  cannot serve as the direct input to neural networks as it lacks meaningful physical representations. In this section, we propose a physically based representation for the 3-tuple  $(d, \theta, \varphi)$ , which we denote as  $\Psi(d, \theta, \varphi)$ . In quantum systems,  $\Psi(d, \theta, \varphi)$  can be treated as the solution to the

Schrödinger equation approximating the DFT.

When investigating the electric structures of molecules, computational models are used to approximate the DFT (Sholl & Steckel, 2011; Calais, 1993). The key proposal of DFT is that the molecular properties are determined by functionals of the spatially dependent electron density. Hence, atomic locations are combined with quantum mechanics to predict properties of molecules. With the electron state expressed as a function of locations as  $\Psi(\mathbf{r})$ , the Schrödinger equation could be written in a time-independent manner as  $-\frac{\hbar^2}{2m} \nabla^2 \Psi(\mathbf{r}) + V(\mathbf{r}) \Psi(\mathbf{r}) = E \Psi(\mathbf{r})$ , where  $m$  denotes the constant mass,  $E$  denotes the constant energy,  $\hbar$  is the reduced Planck constant,  $\nabla^2$  is the Laplacian in the Cartesian coordinate system, and  $V(\mathbf{r})$  is the potential as a function of locations. By performing separation on variables and converting the Cartesian coordinate system to the SCS (Griffiths & Schroeter, 2018), the generic and regular solution to the Schrödinger equation in the SCS is

$$\Psi(d, \theta, \varphi) = \sum_{\ell=0}^{\infty} \sum_{m=-\ell}^{m=\ell} a_{\ell m} j_{\ell}(kd) Y_{\ell}^m(\theta, \varphi), \quad (3)$$

where  $j_{\ell}(\cdot)$  is a spherical Bessel function of order  $\ell$ ,  $Y_{\ell}^m$  is a spherical harmonic function of degree  $m$  and order  $\ell$ , and  $a_{\ell m}$  is the set of coefficients regarding  $\ell$  and  $m$ . In the SMP, we use an orthogonal basis (Cohen et al., 2019; Klicpera et al., 2020b) for  $j_{\ell}(\cdot)$  and set the boundary condition to be  $k = \frac{z_{\ell n}}{c}$ . Thus, we obtain the complete 3D representation for  $(d, \theta, \varphi)$  as

$$\tilde{t}_{\text{BF}, \ell m n}(d, \theta, \varphi) = \sqrt{\frac{2}{c^3 j_{\ell+1}^2(z_{\ell n})}} j_{\ell} \left( \frac{z_{\ell n}}{c} d \right) Y_{\ell}^m(\theta, \varphi), \quad (4)$$

where  $c$  denotes the cutoff,  $z_{\ell n}$  is the  $n$ -th root of the Bessel function of order  $\ell$ . We also have  $\ell \in [0, \dots, N_{\text{SHBF}} - 1]$ ,  $m \in [-\ell, \dots, \ell]$  and  $n \in [1, \dots, N_{\text{SRBF}}]$ .  $N_{\text{SHBF}}$  and  $N_{\text{SRBF}}$  denote the highest orders for the spherical harmonics and spherical Bessel functions, respectively. They are hyperparameters in experimental settings.

We also consider two simplified cases, where we only consider  $d$  and  $\theta$  for the first, and only  $d$  for the second (use a radial basis function). The representations for these two cases can be obtained as

$$\begin{aligned} \tilde{a}_{\text{SBF}, \ell n}(d, \theta) &= \sqrt{\frac{2}{c^3 j_{\ell+1}^2(z_{\ell n})}} j_{\ell} \left( \frac{z_{\ell n}}{c} d \right) Y_{\ell}^0(\theta), \\ \tilde{e}_{\text{RBF}, n}(d) &= \sqrt{\frac{2}{c}} \frac{\sin \left( \frac{n\pi}{c} d \right)}{d}, \end{aligned} \quad (5)$$

where the notations have been defined as in Eq. (4).

### 4.3. SphereNet

Based upon the spherical message passing scheme described in Sec. 4.1 and physical solutions to the DFT in Sec. 4.2, we build the SphereNet for real-world graph data. By incorporating the positional information in spherical coordinates, SphereNet generates predictions that are invariant to translation and rotation of input molecules. Our network is composed of an embedding block, several interaction blocks, and an output block. For clear description, we assume the message  $e^k$  for the edge  $k$  in Fig. 4 and Eq. (2) is the message for update. Specifically, the embedding block generates the initial message for the edge  $k$ , and takes only the distance representation  $\tilde{e}_{\text{RBF},n}(d)$  in Eq. (5) as the input. Each interaction block updates the message for the edge  $k$ . The inputs include messages for all the neighboring edges, and all three representations, including  $\tilde{t}_{\text{BF},\ell mn}(d, \theta, \varphi)$ ,  $\tilde{a}_{\text{SBF},\ell n}(d, \theta)$ , and  $\tilde{e}_{\text{RBF},n}(d)$  in Eq. (4) and Eq. (5) based on the edge  $k$  and its neighboring edges. The output block first takes both the distance representation and the current message for  $k$  as inputs. Then the feature vector of the receiver node for the edge  $k$  (node  $r_k$  in Fig. 4 and Eq. (2)) is obtained by aggregating all the messages pointing to it, where the other messages have a similar update process as  $e^k$ . The detailed architecture for the SphereNet is provided in Appendix A.

## 5. Relations with Prior 3DGN Models

When developing architectures for 3DGN using the sphere message passing, our SphereNet is an advanced model where the relative location of each node is deterministic. The development for 3DGN is still in early stage. To our best knowledge, there exist several notable models in the literature, and they all can be viewed as special cases of the SphereNet, as they capture partial 3D positional information. We describe two exemplary models SchNet and DimeNet in this section. Details of these two models and the description of other models are provided in Appendix B.

### SchNet, Schütt et al. (2017)

SchNet uses continuous-filter convolutional layers to model local correlations for molecules. It essentially incorporates relative distances based on atomic positions. The computational steps for the SchNet are simplified from the SphereNet in Eq. (2) and can be expressed as

$$\begin{aligned} \mathbf{e}'_k &= \varphi^e(\mathbf{v}_{r_k}, \rho^{p \rightarrow e}(\{\mathbf{r}_h\}_{h=r_k \cup s_k})), \\ \mathbf{v}'_i &= \varphi^v(\mathbf{v}_i, \rho^{e \rightarrow v}(E_i)), \\ \mathbf{u}' &= \varphi^u(\rho^{v \rightarrow u}(V')). \end{aligned} \quad (6)$$

As the SchNet only considers the distance information,  $\rho^{p \rightarrow e} = \tilde{e}_{\text{RBF},n}(d)$  in Eq. (5), and  $d$  is the Euclidean distance between the nodes  $r_k$  and  $s_k$ . The other used functions are neural networks or mathematical operations.

### DimeNet, Klicpera et al. (2020b)

DimeNet explicitly includes angles between directed edges in the proposed directional message passing process. Compared with the SchNet, DimeNet moves a step forward by considering both the distance information  $d$  and bond angle information  $\theta$ . As a special case of the SMP defined in Eq. (2), the directional message passing is expressed as

$$\begin{aligned} \mathbf{e}'_k &= \varphi^e\left(\mathbf{e}^k, E_{s_k}, \rho^{p \rightarrow e}\left(\{\mathbf{r}_h\}_{h=r_k \cup s_k \cup \mathcal{N}_{s_k}}\right)\right), \\ \mathbf{v}'_i &= \varphi^v(\mathbf{v}_i, \rho^{e \rightarrow v}(E_i)), \\ \mathbf{u}' &= \varphi^u(\mathbf{u}, \rho^{v \rightarrow u}(V')). \end{aligned} \quad (7)$$

Apparently, in the DimeNet,  $\rho^{p \rightarrow e} = \tilde{a}_{\text{SBF},\ell n}(d, \theta)$  in Eq. (5). The  $d$  and  $\theta$  are illustrated in Fig. 2 and introduced in Sec. 4.1. The other used functions are neural networks or mathematical operations.

## 6. Experimental Studies

### 6.1. Experimental Setup

We apply our SphereNet to three benchmark datasets including QM9 (Ramakrishnan et al., 2014), Open Catalyst 2020 (OC20) (Chaussot et al., 2020), and MD17 (Chmiela et al., 2017). Baseline methods include PPGN (Maron et al., 2019), SchNet (Schütt et al., 2017), PhysNet (Unke & Meuwly, 2019), Cormorant (Anderson et al., 2019), MGNC (Lu et al., 2019), DimeNet (Klicpera et al., 2020b), DimeNet++ (Klicpera et al., 2020a), CGCNN (Xie & Grossman, 2018), and sGML (Chmiela et al., 2018). For all baseline methods, we report the results taken from the referred papers or provided by the original authors. For the SphereNet, all models are trained using stochastic gradient descent (SGD) with the Adam optimizer (Kingma & Ba, 2014). The optimal hyperparameters are obtained by grid search. Network configurations and search space for all models are provided in Appendix C. Code will be released after the anonymous review period.

### 6.2. QM9

We apply the SphereNet to the QM9 dataset, which is widely used for predicting various properties of molecules. It consists organic molecules composed of up to 9 heavy atoms. Thus, this test can examine the power of the SphereNet for similar quantum chemistry systems. The dataset is original split into three sets, where the training set contains 110 000, the validation set contains 10 000, and the test set contains 10 831 molecules. For energy-related properties, the training processes use the unit eV. All hyperparameters are tuned on the validation set and applied to the test set. We compare our SphereNet with baselines using mean absolute error (MAE) for each property and the overall mean standarized MAE (std. MAE) for all the 12 properties. The comparison

Table 1. Comparisons between SphereNet and other models in terms of MAE and the overall mean std. MAE on QM9. ‘-’ denotes no results are reported in the referred papers for the corresponding properties. The best results are shown in bold and the second best results are shown with underlines.

Property	Unit	PPGN	SchNet	PhysNet	Cormorant	MGCN	DimeNet	DimeNet++	<b>SphereNet</b>
$\mu$	D	0.047	0.033	0.0529	0.13	0.0560	<u>0.0286</u>	0.0297	<b>0.0269</b>
$\alpha$	$a_0^{-3}$	0.131	0.235	0.0615	0.092	<b>0.0300</b>	0.0469	<u>0.0435</u>	0.0465
$\epsilon_{\text{HOMO}}$	meV	40.3	41	32.9	36	42.1	27.8	<u>24.6</u>	<b>23.6</b>
$\epsilon_{\text{LUMO}}$	meV	32.7	34	24.7	36	57.4	19.7	<u>19.5</u>	<b>18.9</b>
$\Delta\epsilon$	meV	60.0	63	42.5	60	64.2	34.8	<u>32.6</u>	<b>32.3</b>
$\langle R^2 \rangle$	$a_0^{-2}$	0.592	<b>0.073</b>	0.765	0.673	<u>0.110</u>	0.331	0.331	0.292
ZPVE	meV	3.12	1.7	1.39	1.98	<b>1.12</b>	1.29	<u>1.21</u>	<b>1.12</b>
$U_0$	meV	36.8	14	8.15	28	12.9	8.02	<u>6.32</u>	<b>6.26</b>
$U$	meV	36.8	19	8.34	-	14.4	7.89	<b>6.28</b>	<u>7.33</u>
$H$	meV	36.3	14	8.42	-	14.6	8.11	<u>6.53</u>	<b>6.40</b>
$G$	meV	36.4	14	9.40	-	16.2	8.98	<b>7.56</b>	<u>8.0</u>
$c_v$	$\frac{\text{cal}}{\text{mol K}}$	0.055	0.033	0.0280	0.031	0.0380	0.0249	0.0230	<b>0.0215</b>
std. MAE	%	1.84	1.76	1.37	2.14	1.86	1.05	<u>0.98</u>	<b>0.94</b>

Table 2. Comparisons between SphereNet and other models on IS2RE in terms of energy MAE and the percentage of EwT of the ground truth energy. Results reported for models trained on the training set with size of 10k. The best results are shown in bold.

Model	Energy MAE [eV] ↓				EwT ↑			
	ID	OOD Ads	OOD Cat	OOD Both	ID	OOD Ads	OOD Cat	OOD Both
CGCNN	1.0479	1.0527	1.0232	0.9608	1.39%	1.38%	1.59%	1.57%
SchNet	1.0858	1.1044	1.0720	1.0391	1.34%	1.39%	1.42%	1.44%
DimeNet	1.0117	1.0734	0.9814	0.9767	1.45%	1.41%	1.53%	1.41%
DimeNet++	0.8819	0.9106	0.8357	0.8408	1.94%	1.69%	2.13%	1.84%
<b>SphereNet</b>	<b>0.8352</b>	<b>0.8723</b>	<b>0.7959</b>	<b>0.7952</b>	<b>1.96%</b>	<b>2.02%</b>	<b>2.19%</b>	<b>1.90%</b>

results are summarized in Table 1. SphereNets achieves best performance on 8 properties and the second best performance on 2 properties. It also sets the new state of the art on the overall mean std. MAE of the QM9 dataset.

### 6.3. OC20

The Open Catalyst 2020 (OC20) dataset is a newly released large-scale dataset for catalyst discovery and optimization (Chanussot et al., 2020). It comprises millions of DFT relaxations across huge chemical structure space such that machine learning models can be fully trained. There exist three tasks including S2EF, IS2RS, and IS2RE. In this work, we focus on IS2RE that predicts structure’s energy in the relaxed state. It is the most common task in catalysis as relaxed energies usually influence the catalyst activity. The dataset for IS2RE is originally split into training/validation/test sets. The test label is not publicly available. Experiments are conducted on the validation set, which has four splits including In Domain (ID), Out of Domain Adsorbates (OOD Ads), Out of Domain catalysts (OOD cat), and Out of Domain Adsorbates and catalysts (OOD Both), where numbers of samples are 24 943, 24 961,

24 963, 24 987, respectively. Results for all the baselines are provided by the original authors, and we report evaluation results of fixed epochs for SphereNet. Following a setting in Chanussot et al. (2020), we use the training set with size 10k for training models. The used metrics are the energy MAE and the percentage of Energies within a Threshold (EwT) of the ground truth energy. Table 2 shows that the SphereNet consistently achieves the best performance on all the four splits in terms of energy MAE and EwT. It reduces the average energy MAE on four splits by 0.043, which is 4.91% of the second best model. In addition, it improves the average EwT from 1.90% to 2.02%, which is a large margin considering the inherently low EwT values.

### 6.4. MD17

The MD17 dataset is used to examine the expressive power of SphereNet for molecular dynamics simulations. The goal is to predict energy-conserving forces at the atomic level for eight organic molecules, each of which has hundreds of thousands states simulated by DFT and atom coordinates. Following the settings in Schütt et al. (2017); Klicpera et al. (2020b), we train a separate model for each molecule to

Table 3. Comparisons between SphereNets and other models in terms MAE of forces on MD17. The best results are shown in bold and the second best results are shown with underlines.

Molecule	sGDML	SchNet	DimeNet	<b>SphereNet</b>
Aspirin	0.68	1.35	<u>0.499</u>	<b>0.430</b>
Benzene	0.20	0.31	<u>0.187</u>	<b>0.178</b>
Ethanol	0.33	0.39	<u>0.230</u>	<b>0.208</b>
Malonaldehyde	0.41	0.66	<u>0.383</u>	<b>0.340</b>
Naphthalene	<b>0.11</b>	0.58	0.215	0.178
Salicylic acid	<b>0.28</b>	0.85	0.374	0.360
Toluene	<b>0.14</b>	0.57	0.216	<u>0.155</u>
Uracil	<b>0.24</b>	0.56	0.301	0.267
std. MAE	1.11	2.38	<u>1.10</u>	<b>0.97</b>

Table 4. Comparisons among three message passing strategies on the same SphereNet architecture on the partial MD17 dataset.

Molecule	SMP w/o $(\theta, \varphi)$	SMP w/o $\varphi$	SMP
Ethanol	0.249	0.22	0.208
Malonaldehyde	0.550	0.360	0.340
Naphthalene	0.372	0.205	0.178
Toluene	0.446	0.182	0.155

predict atomic forces. We use 1000 samples for training, and each of the eight molecules has both the validation and test sets. Hyperparameters are tuned on validation sets and applied to test sets. The results for forces are reported in Table 3. Results for baselines are taken from referred papers and there are no original results for DimeNet++. Note that for Benzene, all models are evaluated on Benzene17, thus, the result for sGDML is 0.20 rather than 0.06 (Benzene18). We can observe from the table that SphereNet consistently outperforms SchNet and DimeNet by largin margins. Compared with sGDML, SphereNet performs better on four molecules, and achieves much better std. MAE with 0.97. sGDML is one of the original work that created the MD17 dataset with carefully-designed features, thus, it naturally has advantages for small molecules. However, compared with SphereNet, sGDML has poorer generalization power to larger datasets without hand-engineered features.

## 6.5. Ablation Study

The proposed SMP considers all the distance, angle, and torsion information, leading to complete representations of 3D information. In this section, we investigate contributions of different 3D information to demonstrate the advances of our SMP. We remove torsion information from SMP which we denote as “SMP w/o  $\varphi$ ”; we further remove angle information which we denote as “SMP w/o  $(\theta, \varphi)$ ”. The three message passing strategies are integrated to the same architecture with other network parts remaining the same. We evaluate these models on four molecules of MD17. Table 4

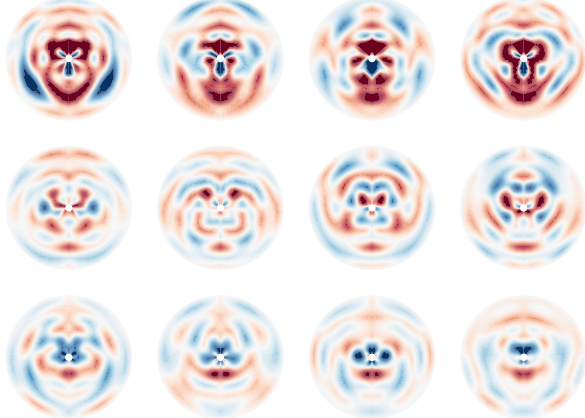


Figure 6. Visualization of three SphereNet filters. Each row corresponds to a filter with torsion angles 0,  $\pi/2$ ,  $\pi$ , and  $3\pi/2$  from left to right.

Table 5. Efficiency comparisons between SphereNet and other models in terms of number of parameters and time cost per epoch using the same infrastructure.

	SchNet	DimeNet	DimeNet++	SphereNet
#Param.	185 153	2100 070	1887 110	1898 566
Time (s)	100	840	240	340

shows that SMP outperforms SMP w/o  $\varphi$ , and SMP w/o  $\varphi$  outperforms “SMP w/o  $(\theta, \varphi)$ ”. These results demonstrate the effectiveness of angle and torsion information used in the SMP. The best performance of SMP further reveals that SMP represents an accurate architecture for realizing the 3DGN framework. Fig. 6 provides the visualization of filters in a learned SphereNet model. Among the distance, angle and torsion, considering any one when fixing the other two, the structural value of filters will be different when the one of interest changes. It essentially shows that all the distance, angle, and torsion information determine the structural semantics of filters. This further demonstrates that SMP enables the learning of different 3D information for improving representations. Details of the SphereNet filters and more visualization results are provided in Appendix D.

## 6.6. Efficiency Study of SphereNet

Since SphereNet computes geometries such as torsion angles, and employs linear layers for incorporating 3D information, it involves extra parameters and computational resources. We study the efficiency of SphereNet by comparing with other models regarding number of parameters and time cost per epoch using the same computing infrastructure (Nvidia GeForce RTX 2080 TI 11GB). Experiments are conducted on the property  $U_0$  of QM9 and results are shown in Table 5. It is obvious that SphereNet uses similar computational resources as DimeNet++, and is much more efficient than DimeNet.

## 7. Conclusion

3D information is important for real-world graph data but the existing GN framework does not consider it. We first build the generic and unified framework 3DGN to provide a clear interface for 3D graphs. We further develop a novel message passing architecture SMP for realizing the 3DGN, and show that SMP represents a complete and accurate architecture in SCS. Based on SMP and meaningful physical representations, SphereNet is presented for real-world 3D graph data. Experimental results on various types of datasets show that SphereNet leads to significant performance improvements without increasing computations.

## Acknowledgments

This work was supported in part by National Science Foundation grant IIS-1908198 and National Institutes of Health grant 1R21NS102828.

## References

Anderson, B., Hy, T.-S., and Kondor, R. Cormorant: Covariant molecular neural networks. In *Proceedings of the 33st International Conference on Neural Information Processing Systems*, pp. 14537–14546, 2019.

Axelrod, S. and Gomez-Bombarelli, R. Geom: Energy-annotated molecular conformations for property prediction and molecular generation. *arXiv preprint arXiv:2006.05531*, 2020.

Battaglia, P. W., Hamrick, J. B., Bapst, V., Sanchez-Gonzalez, A., Zambaldi, V., Malinowski, M., Tacchetti, A., Raposo, D., Santoro, A., Faulkner, R., et al. Relational inductive biases, deep learning, and graph networks. *arXiv preprint arXiv:1806.01261*, 2018.

Calais, J.-L. Density-functional theory of atoms and molecules. rg parr and w. yang, oxford university press, new york, oxford, 1989. ix+ 333 pp. price£ 45.00. *International Journal of Quantum Chemistry*, 47(1):101–101, 1993.

Chanussot, L., Das, A., Goyal, S., Lavril, T., Shuaibi, M., Riviere, M., Tran, K., Heras-Domingo, J., Ho, C., Hu, W., et al. The open catalyst 2020 (oc20) dataset and community challenges. *arXiv preprint arXiv:2010.09990*, 2020.

Chmiela, S., Tkatchenko, A., Sauceda, H. E., Poltavsky, I., Schütt, K. T., and Müller, K.-R. Machine learning of accurate energy-conserving molecular force fields. *Science advances*, 3(5):e1603015, 2017.

Chmiela, S., Sauceda, H. E., Müller, K.-R., and Tkatchenko, A. Towards exact molecular dynamics simulations with machine-learned force fields. *Nature communications*, 9(1):1–10, 2018.

Cohen, T., Weiler, M., Kicanaoglu, B., and Welling, M. Gauge equivariant convolutional networks and the icosahedral cnn. In *International Conference on Machine Learning*, pp. 1321–1330, 2019.

Defferrard, M., Bresson, X., and Vandergheynst, P. Convolutional neural networks on graphs with fast localized spectral filtering. *Advances in neural information processing systems*, 29:3844–3852, 2016.

Fout, A., Byrd, J., Shariat, B., and Ben-Hur, A. Protein interface prediction using graph convolutional networks. In *Proceedings of the 31st International Conference on Neural Information Processing Systems*, pp. 6533–6542, 2017.

Gao, H. and Ji, S. Graph U-nets. In *Proceedings of The 36th International Conference on Machine Learning*, pp. 2083–2092, 2019.

Gao, H., Wang, Z., and Ji, S. Large-scale learnable graph convolutional networks. In *Proceedings of the 24th ACM SIGKDD International Conference on Knowledge Discovery and Data Mining*, pp. 1416–1424, 2018.

Gao, H., Liu, Y., and Ji, S. Topology-aware graph pooling networks. *arXiv preprint arXiv:2010.09834*, 2020.

Garg, V., Jegelka, S., and Jaakkola, T. Generalization and representational limits of graph neural networks. In *International Conference on Machine Learning*, pp. 3419–3430, 2020.

Gilmer, J., Schoenholz, S. S., Riley, P. F., Vinyals, O., and Dahl, G. E. Neural message passing for quantum chemistry. In *Proceedings of the 34th International Conference on Machine Learning-Volume 70*, pp. 1263–1272. JMLR.org, 2017.

Gori, M., Monfardini, G., and Scarselli, F. A new model for learning in graph domains. In *Proceedings. 2005 IEEE International Joint Conference on Neural Networks, 2005.*, volume 2, pp. 729–734. IEEE, 2005.

Griffiths, D. J. and Schroeter, D. F. *Introduction to quantum mechanics*. Cambridge University Press, 2018.

Hamilton, W., Ying, Z., and Leskovec, J. Inductive representation learning on large graphs. In *Advances in neural information processing systems*, pp. 1024–1034, 2017.

Ingraham, J., Garg, V. K., Barzilay, R., and Jaakkola, T. Generative models for graph-based protein design. In *Advances in Neural Information Processing Systems*, pp. 15794–15805, 2019.

Kingma, D. P. and Ba, J. Adam: A method for stochastic optimization. *arXiv preprint arXiv:1412.6980*, 2014.

Kipf, T. N. and Welling, M. Semi-supervised classification with graph convolutional networks. In *International Conference on Learning Representations*, 2017.

Klicpera, J., Giri, S., Margraf, J. T., and Günnemann, S. Fast and uncertainty-aware directional message passing for non-equilibrium molecules. In *NeurIPS-W*, 2020a.

Klicpera, J., Groß, J., and Günnemann, S. Directional message passing for molecular graphs. In *International Conference on Learning Representations (ICLR)*, 2020b.

Li, Y., Tarlow, D., Brockschmidt, M., and Zemel, R. Gated graph sequence neural networks. In *International Conference on Learning Representations*, 2016.

Liu, S., Demirel, M. F., and Liang, Y. N-gram graph: Simple unsupervised representation for graphs, with applications to molecules. *Advances in Neural Information Processing Systems*, 32:8464–8476, 2019.

Liu, Y., Yuan, H., Cai, L., and Ji, S. Deep learning of high-order interactions for protein interface prediction. In *Proceedings of the 26th ACM SIGKDD International Conference on Knowledge Discovery & Data Mining*, pp. 679–687, 2020.

Lu, C., Liu, Q., Wang, C., Huang, Z., Lin, P., and He, L. Molecular property prediction: A multilevel quantum interactions modeling perspective. In *Proceedings of the AAAI Conference on Artificial Intelligence*, volume 33, pp. 1052–1060, 2019.

Maron, H., Ben-Hamu, H., Serviansky, H., and Lipman, Y. Provably powerful graph networks. *Advances in Neural Information Processing Systems*, 32:2153–2164, 2019.

Qiao, Z., Welborn, M., Anandkumar, A., Manby, F. R., and Miller III, T. F. Orbnet: Deep learning for quantum chemistry using symmetry-adapted atomic-orbital features. *The Journal of Chemical Physics*, 153(12):124111, 2020.

Ramakrishnan, R., Dral, P. O., Rupp, M., and Von Lilienfeld, O. A. Quantum chemistry structures and properties of 134 kilo molecules. *Scientific data*, 1(1):1–7, 2014.

Sanchez-Gonzalez, A., Godwin, J., Pfaff, T., Ying, R., Leskovec, J., and Battaglia, P. Learning to simulate complex physics with graph networks. In *International Conference on Machine Learning*, pp. 8459–8468, 2020.

Scarselli, F., Gori, M., Tsoi, A. C., Hagenbuchner, M., and Monfardini, G. The graph neural network model. *IEEE transactions on neural networks*, 20(1):61–80, 2008.

Schütt, K., Kindermans, P.-J., Felix, H. E. S., Chmiela, S., Tkatchenko, A., and Müller, K.-R. Schnet: A continuous-filter convolutional neural network for modeling quantum interactions. In *Advances in neural information processing systems*, pp. 991–1001, 2017.

Shervashidze, N., Schweitzer, P., Van Leeuwen, E. J., Mehlhorn, K., and Borgwardt, K. M. Weisfeiler-lehman graph kernels. *Journal of Machine Learning Research*, 12(9), 2011.

Sholl, D. and Steckel, J. A. *Density functional theory: a practical introduction*. John Wiley & Sons, 2011.

Simm, G., Pinsler, R., and Hernández-Lobato, J. M. Reinforcement learning for molecular design guided by quantum mechanics. In *International Conference on Machine Learning*, pp. 8959–8969, 2020.

Townshend, R., Bedi, R., Suriana, P., and Dror, R. End-to-end learning on 3d protein structure for interface prediction. *Advances in Neural Information Processing Systems*, 32:15642–15651, 2019.

Unke, O. T. and Meuwly, M. Physnet: A neural network for predicting energies, forces, dipole moments, and partial charges. *Journal of chemical theory and computation*, 15(6):3678–3693, 2019.

Veličković, P., Cucurull, G., Casanova, A., Romero, A., Lio, P., and Bengio, Y. Graph attention networks. In *International Conference on Learning Representations*, 2018.

Vignac, C., Loukas, A., and Frossard, P. Building powerful and equivariant graph neural networks with message-passing. *arXiv preprint arXiv:2006.15107*, 2020.

Wang, Z., Liu, M., Luo, Y., Xu, Z., Xie, Y., Wang, L., Cai, L., and Ji, S. Advanced graph and sequence neural networks for molecular property prediction and drug discovery. *arXiv preprint arXiv:2012.01981*, 2020.

Wu, Z., Ramsundar, B., Feinberg, E. N., Gomes, J., Geniesse, C., Pappu, A. S., Leswing, K., and Pande, V. Moleculenet: a benchmark for molecular machine learning. *Chemical science*, 9(2):513–530, 2018.

Xie, T. and Grossman, J. C. Crystal graph convolutional neural networks for an accurate and interpretable prediction of material properties. *Physical review letters*, 120(14):145301, 2018.

Xu, K., Hu, W., Leskovec, J., and Jegelka, S. How powerful are graph neural networks? In *International Conference on Learning Representations*, 2019.

Yuan, H. and Ji, S. StructPool: Structured graph pooling via conditional random fields. In *Proceedings of the 8th International Conference on Learning Representations*, 2020.

Zhang, M., Cui, Z., Neumann, M., and Chen, Y. An end-to-end deep learning architecture for graph classification. In *Proceedings of the AAAI Conference on Artificial Intelligence*, volume 32, 2018.

## Spherical Message Passing for 3D Graph Networks: Appendix

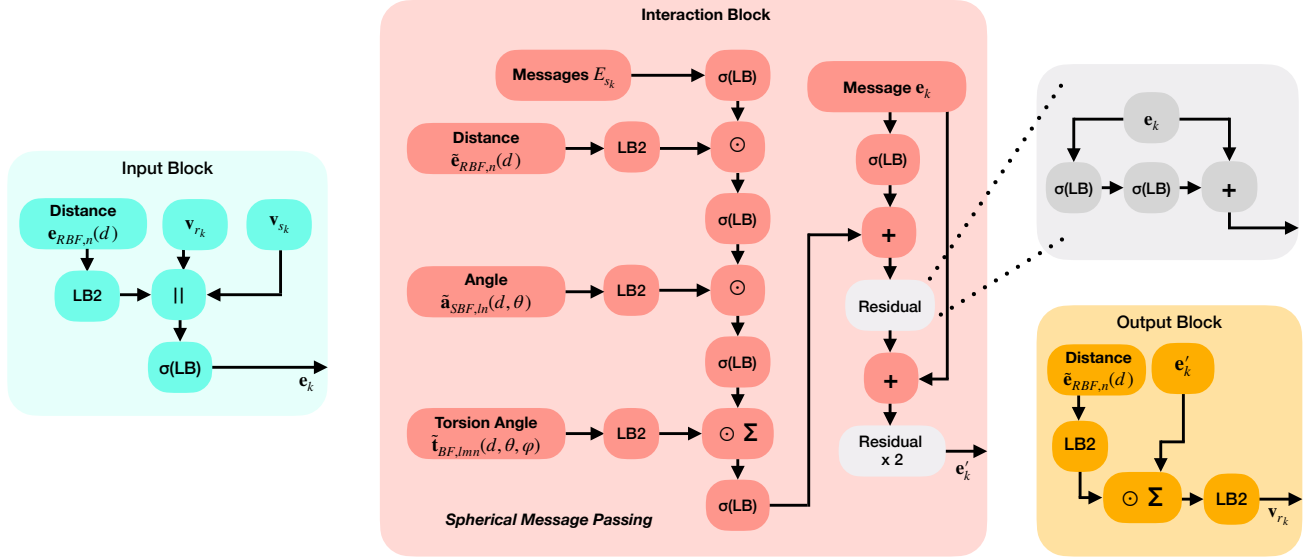


Figure 7. Architecture of SphereNet. LB2 denotes a linear block with two linear layers,  $\sigma(\text{LB})$  denotes a linear layer followed by an activation function,  $\parallel$  denotes concatenation, and  $\odot$  denotes element-wise multiplication. Each LB2 aims at canceling bottlenecks by performing downprojection, followed by upprojection. Hence, it is related to three hyperparameters: these are, input embedding size, intermediate size, and output embedding size. Each linear block LB is related to hyperparameters including input embedding size and output embedding size. Description of each block is in Sec. A.

### A. Architecture of SphereNet

The architecture of SphereNet is designed based on DimeNet++ (Klicpera et al., 2020a), where we incorporate our proposed spherical message passing and the torsion representation  $\tilde{t}_{\text{BF},\ell mn}(d, \theta, \varphi)$ . Detailed architecture of SphereNet is provided in Fig. 7. Specifically, SphereNet is composed of an input block, followed by multiple interaction blocks and an output block. For the purpose of simplicity, the architecture is explained by updating the receiver node  $r_k$  of the message  $\mathbf{e}_k$ , as described in Eq. 2 and Sec. 4.3 in main paper.

**Input Block** aims at constructing initial message  $\mathbf{e}_k$  for the edge  $k$ . Inputs include the distance representation  $\tilde{e}_{\text{RBF},n}(d)$  for edge  $k$ , initial node embeddings  $\mathbf{v}_{s_k}, \mathbf{v}_{r_k}$  for the sender node  $s_k$ , and the receiver node  $r_k$ . The distance information is encoded by using a LB2 block.

**Interaction Block** updates the message  $\mathbf{e}_k$  with incorporating all the three physical representations. Input 3D information includes the distance embedding  $\tilde{e}_{\text{RBF},n}(d)$ , the angle  $\tilde{a}_{\text{SBF},ln}(d, \theta)$ , and the torsion  $\tilde{t}_{\text{BF},\ell mn}(d, \theta, \varphi)$ . The initial embedding sizes for them are  $N_{\text{SHBF}}, N_{\text{SRBF}} \times N_{\text{SHBF}}$ , and  $N_{\text{SRBF}}^2 \times N_{\text{SHBF}}$ , respectively. Other inputs are old message  $\mathbf{e}_k$  and the set of messages  $E_{s_k}$  that point to the sender node  $s_k$ . Similar to the input block, each type of 3D information is encoded by using a block LB2. Note that each  $\odot$  indicates the element-wise multiplication between the corresponding 3D information represented as a vector and each message in the set  $E_{s_k}$ . Thus, each neighboring message of  $\mathbf{e}_k$  is gated by the encoded 3D information. The  $\sum$  aggregates all the gated messages in  $E_{s_k}$  to a vector, which is added to the transformation of the old message  $\mathbf{e}_k$  as the updated message  $\mathbf{e}'_k$ . The transformation branch for old message  $\mathbf{e}_k$  is composed of several nonlinear layers and residual blocks, as shown in Fig. 7.

**Output Block** aggregates all the incoming messages to update the feature for node  $r_k$ . Each incoming message has the same update process as  $\mathbf{e}_k$  by interaction blocks. For the purpose of clear illustration, we use  $\mathbf{e}'_k$  to represent each updated incoming message, which is further gated by the distance representation vector  $\tilde{e}_{\text{RBF},n}(d)$ .

## B. Relations with Prior 3DGN Models

### B.1. SchNet, Schütt et al. (2017)

In SchNet, the used aggregation function to encode 3D positional information is  $\rho^{p \rightarrow e}(\{\mathbf{r}_h\}_{h=r_k \cup s_k}) = \tilde{e}_{\text{RBF},n}(\|\mathbf{r}_{r_k} - \mathbf{r}_{s_k}\|)$ , which converts the positional information to an embedding of distance. In addition to the  $\rho^{p \rightarrow e}$  function, the  $\phi^e$  function used is  $\text{NN}(\text{NN}(\mathbf{v}_{r_k}) \odot \text{NN}(\tilde{e}_{\text{RBF},n}(\|\mathbf{r}_{r_k} - \mathbf{r}_{s_k}\|)))$ , where  $\text{NN}$  denotes a neural network and  $\odot$  denotes the element-wise multiplication. The  $\rho^{e \rightarrow v}$  function is  $\sum_{(\mathbf{e}'_k, r_k, s_k) \in E_i} \mathbf{e}'_k$ . The  $\phi^v$  function is  $\mathbf{v}_i + \sum_{(\mathbf{e}'_k, r_k, s_k) \in E_i} \mathbf{e}'_k$ . The global feature  $\mathbf{u}$  is updated based on the final node features  $V^T$  and the function is  $\phi^u = \sum_{i=1:n} \text{NN}(\mathbf{v}_i^T)$ . Formally, the update process is expressed as

$$\begin{aligned}
 \mathbf{e}'_k &= \phi^e(\mathbf{v}_{r_k}, \rho^{p \rightarrow e}(\{\mathbf{r}_h\}_{h=r_k \cup s_k})) \\
 &= \phi^e(\mathbf{v}_{r_k}, \tilde{e}_{\text{RBF},n}(\|\mathbf{r}_{s_k} - \mathbf{r}_{r_k}\|)) \\
 &= \text{NN}(\text{NN}(\mathbf{v}_{r_k}) \odot \text{NN}(\tilde{e}_{\text{RBF},n}(\|\mathbf{r}_{r_k} - \mathbf{r}_{s_k}\|))), \\
 \mathbf{v}'_i &= \phi^v(\mathbf{v}_i, \rho^{e \rightarrow v}(E_i)) \\
 &= \phi^v\left(\mathbf{v}_i, \sum_{(\mathbf{e}'_k, r_k, s_k) \in E_i} \mathbf{e}'_k\right) \\
 &= \mathbf{v}_i + \sum_{(\mathbf{e}'_k, r_k, s_k) \in E_i} \mathbf{e}'_k, \\
 \mathbf{u} &= \phi^u(\rho^{v \rightarrow u}(V^T)) \\
 &= \sum_{i=1:n} \text{NN}(\mathbf{v}_i^T).
 \end{aligned} \tag{8}$$

### B.2. PhysNet, Unke & Meuwly (2019)

PhysNet uses distance between atoms as an important feature and proposes more powerful neural networks for chemical applications. The positional aggregation function is  $\rho^{p \rightarrow e}(\{\mathbf{r}_h\}_{h=r_k \cup s_k}) = \mathbf{g}(\|\mathbf{r}_{r_k} - \mathbf{r}_{s_k}\|)$ , where  $\mathbf{g}$  is any radial basis function with a smooth cutoff. For the information update functions, the  $\phi^e$  function is  $\sigma(\mathbf{W}_1) \sigma(\mathbf{v}_{s_k}) \odot \mathbf{W}_2 \mathbf{g}(\|\mathbf{r}_{r_k} - \mathbf{r}_{s_k}\|)$ , the  $\phi^v$  function is  $\text{NN}(\mathbf{W}_3 \odot \mathbf{v}_i + \text{NN}(\sigma(\mathbf{W}_4) \sigma(\mathbf{v}_i) + \sum_{(\mathbf{e}'_k, r_k, s_k) \in E_i} \mathbf{e}'_k))$  and the  $\phi^u$  function is  $\mathbf{u} + \sum_{i=1:n} \text{NN}(\mathbf{v}'_i)$ . Here  $\text{NN}$  denotes a neural network,  $\mathbf{W}_1, \mathbf{W}_2, \mathbf{W}_3, \mathbf{W}_4$  are learnable weight matrices,  $\sigma$  is an activate function, and  $\odot$  denotes the element-wise multiplication. PhysNet is expressed as

$$\begin{aligned}
 \mathbf{e}'_k &= \phi^e(\mathbf{v}_{s_k}, \rho^{p \rightarrow e}(\{\mathbf{r}_h\}_{h=r_k \cup s_k})) \\
 &= \phi^e(\mathbf{v}_{s_k}, \mathbf{g}(\|\mathbf{r}_{r_k} - \mathbf{r}_{s_k}\|)) \\
 &= \sigma(\mathbf{W}_1) \sigma(\mathbf{v}_{s_k}) \odot \mathbf{W}_2 \mathbf{g}(\|\mathbf{r}_{r_k} - \mathbf{r}_{s_k}\|), \\
 \mathbf{v}'_i &= \phi^v(\mathbf{v}_i, \rho^{e \rightarrow v}(E_i)) \\
 &= \phi^v\left(\mathbf{v}_i, \sum_{(\mathbf{e}'_k, r_k, s_k) \in E_i} \mathbf{e}'_k\right) \\
 &= \text{NN}\left(\mathbf{W}_3 \odot \mathbf{v}_i + \text{NN}\left(\sigma(\mathbf{W}_4) \sigma(\mathbf{v}_i) + \sum_{(\mathbf{e}'_k, r_k, s_k) \in E_i} \mathbf{e}'_k\right)\right), \\
 \mathbf{u}' &= \phi^u(\rho^{v \rightarrow u}(V'), \mathbf{u}) \\
 &= \mathbf{u} + \sum_{i=1:n} \text{NN}(\mathbf{v}'_i).
 \end{aligned} \tag{9}$$

### B.3. DimeNet, Klicpera et al. (2020b)

DimeNet explicitly considers distances between atoms and angles between directed edges. The aggregation functions on the positional information is  $\rho^{p \rightarrow e} = (\tilde{e}_{\text{RBF},n} \| \tilde{a}_{\text{SBF},\ell n})$ , where  $\|$  denotes concatenation. For other functions, the  $\phi^e$  function used is  $\mathbf{e}'_k = (\mathbf{e}'_{k,1} \| \mathbf{e}'_{k,2})$  with  $\mathbf{e}'_{k,1} = \text{NN} \left( \mathbf{e}_{k,1} + \text{NN} \left( \sigma \mathbf{W}_1 \mathbf{e}_{k,1} + \sum_{(\mathbf{e}_j, r_j, s_j) \in E_{s_k}} \mathbf{W}_2 \tilde{a}_{\text{SBF},\ell n}^{k,j} (\mathbf{W}_3 \tilde{e}_{\text{RBF},n}^j \odot \sigma \mathbf{W}_4 \mathbf{e}_{j,1}) \right) \right)$  and  $\mathbf{e}'_{k,2} = \mathbf{W}_5 \tilde{e}_{\text{RBF},n}^j \odot \mathbf{e}'_{k,1}$ , where NN denotes a neural network,  $\mathbf{W}_1, \mathbf{W}_2, \mathbf{W}_3, \mathbf{W}_4, \mathbf{W}_5$  are different weight matrices, and  $\sigma$  is an activation function. The  $\rho^{e \rightarrow v}$  function is  $\sum_{(\mathbf{e}'_k, r_k, s_k) \in E_i} \mathbf{e}'_{k,2}$  and the  $\phi^v$  is  $\text{NN} \left( \sum_{(\mathbf{e}'_k, r_k, s_k) \in E_i} \mathbf{e}'_{k,2} \right)$ . The  $\rho^{v \rightarrow u}$  is  $\sum_{i=1:n} \mathbf{v}'_i$  and the  $\phi^u$  is  $\mathbf{u} + \sum_{i=1:n} \mathbf{v}'_i$ . Note that  $\rho^{p \rightarrow v}$ ,  $\rho^{p \rightarrow u}$ ,  $\rho^{e \rightarrow u}$  functions are not required in DimeNet. The whole model is expressed as

$$\begin{aligned}
 \mathbf{e}_k &= (\mathbf{e}_{k,1} \| \mathbf{e}_{k,2}), \\
 \rho^{p \rightarrow e} &= (\tilde{e}_{\text{RBF},n} \| \tilde{a}_{\text{SBF},\ell n}), \\
 \mathbf{e}'_{k,1} &= \phi^e \left( \mathbf{e}_k, E_{s_k}, \rho^{p \rightarrow e} \left( \{\mathbf{r}_h\}_{h=r_k \cup s_k \cup \mathcal{N}_{s_k}} \right) \right) \\
 &= \text{NN} \left( \mathbf{e}_{k,1} + \text{NN} \left( \sigma \mathbf{W}_1 \mathbf{e}_{k,1} + \sum_{(\mathbf{e}_j, r_j, s_j) \in E_{s_k}} \mathbf{W}_2 \tilde{a}_{\text{SBF},\ell n}^{k,j} (\mathbf{W}_3 \tilde{e}_{\text{RBF},n}^j \odot \sigma \mathbf{W}_4 \mathbf{e}_{j,1}) \right) \right), \\
 \mathbf{e}'_{k,2} &= \mathbf{W}_5 \tilde{e}_{\text{RBF},n}^j \odot \mathbf{e}'_{k,1}, \\
 \mathbf{v}'_i &= \phi^v (\rho^{e \rightarrow v} (E_i)) \\
 &= \text{NN} \left( \sum_{(\mathbf{e}'_k, r_k, s_k) \in E_i} \mathbf{e}'_{k,2} \right), \\
 \mathbf{u}' &= \phi^u (\mathbf{u}, \rho^{v \rightarrow u} (V')) \\
 &= \mathbf{u} + \sum_{i=1:n} \mathbf{v}'_i.
 \end{aligned} \tag{10}$$

## C. Experimental Setup

For all the models used in three datasets, we set input embedding size = 256 and output embedding size = 64 for both LB2 and LB blocks. For each separate model, we first perform warmup on initial learning rate. Then two learning rate strategies, including CosineAnnealingLR and StepLR, are used for training. For StepLR, the learning rate is decayed by the decay ratio every fixed epochs represented as step size. We do not use weight decay or dropout for all models. For MD17, we follow the settings in Klicpera et al. (2020b); Schütt et al. (2017) and use a joint loss of forces and conserved energy during training. The forces' weight is set to be 100 for all models. Some hyperparameters are fixed values, and some are tuned by grid search. Values/search space of hyperparameters for OC20, QM9, and MD17 are provided in Table 6, Table 7, and Table 8, respectively. As described in main paper, optimized hyperparameters are tuned on validation sets and applied to test sets for QM9 and MD17. For OC20, optimized hyperparameters are obtained on the ID split within max epochs, and then applied to the other three splits. Pytorch is used to implement all methods. For QM9 and MD17 datasets, all models are trained using one NVIDIA GeForce RTX 2080 Ti 11GB GPU. For the OC20 dataset, all models are trained using four NVIDIA Tesla V100 32GB GPUs.

## D. SphereNet Filter Visualization

We visualize SphereNet filters from a learned SphereNet model. Specifically, we port learned weights for the block LB2 after the torsion embedding  $\tilde{t}_{\text{BF},\ell mn}(d, \theta, \varphi)$  in Fig. 7. For each location represented by a tuple  $(d, \theta, \varphi)$ , the initial embedding size is  $N_{\text{SRBF}}^2 \times N_{\text{SHBF}}$ . The computation for the above LB2 is  $\mathbf{W}_1 (\mathbf{W}_2 \tilde{t}_{\text{BF},\ell mn}(d, \theta, \varphi))$ , which results in the new embedding size of 64 for each location  $(d, \theta, \varphi)$ . We then perform sampling on locations in 3D space for visualizing weights as SphereNet filters. We set sampling rate in the torsion direction to be  $\pi/2$  in Fig. 6, and a smaller rate  $\pi/4$  in Fig. 8. Thus, there are four samples in the torsion direction in Fig. 6 and eight samples in Fig. 8. For the distance and angle directions, we use much smaller sample rates to provide visualization maps with high resolution. There are totally 64 elements for each location, and we randomly pick 6 elements as shown in Fig. 8.

Table 6. Values/search space for hyperparameters on OC20.

Hyperparameters	Values/search space
Interaction block - distance LB2 intermediate size	8
Interaction block - angle LB2 intermediate size	8
Interaction block - torsion LB2 intermediate size	8
# of interaction blocks	3, 4
# of RBFs $N_{\text{SRBF}}$	6
# of spherical harmonics $N_{\text{SHBF}}$	7
Cutoff distance	5, 6
Batch size	16, 32
Initial learning rate	1e-4, 5e-4, 1e-3
Learning rate strategy	CosineAnnealingLR, StepLR
T_max (for CosineAnnealingLR)	Max # of Epochs
Learning rate decay ratio (for StepLR)	0.1, 0.4, 0.6
Learning rate step size (for StepLR)	10
Learning rate warmup epochs	3
Learning rate warmup factor	0.2
Max # of Epochs	20, 30, 50

Figure 8. Visualization of six SphereNet filters. Each row corresponds to a filter with torsion angles  $0, \pi/4, \pi/2, 3\pi/4, \pi, 5\pi/4, 3\pi/2$ , and  $7\pi/4$  from left to right.

Table 7. Values/search space for hyperparameters on QM9.

Hyperparameters	Values/search space
Interaction block - distance LB2 intermediate size	4, 8, 16
Interaction block - angle LB2 intermediate size	4, 8, 16
Interaction block - torsion LB2 intermediate size	4, 8, 16
# of interaction blocks	3, 4, 5
# of RBFs $N_{SRBF}$	6
# of spherical harmonics $N_{SHBF}$	7
Cutoff distance	4, 5, 6
Batch size	32, 64
Initial learning rate	1e-4, 5e-4, 1e-3
Learning rate strategy	StepLR
Learning rate decay ratio	0.1, 0.4, 0.5, 0.6
Learning rate step size	30, 50, 100
Learning rate warmup epochs	2, 3, 4
Learning rate warmup factor	0.2
Max # of Epochs	100, 300, 500

Table 8. Values/search space for hyperparameters on MD17.

Hyperparameters	Values/search space
Interaction block - distance LB2 intermediate size	4, 8, 16
Interaction block - angle LB2 intermediate size	4, 8, 16
Interaction block - torsion LB2 intermediate size	4, 8, 16
# of interaction blocks	2, 3, 4, 5
# of RBFs $N_{SRBF}$	6
# of spherical harmonics $N_{SHBF}$	7
Cutoff distance	4, 5, 6
Batch size	4, 16, 32
Initial learning rate	1e-4, 5e-4, 1e-3
Learning rate strategy	StepLR
Learning rate decay ratio	0.1, 0.4, 0.5, 0.6
Learning rate step size	30, 50, 100, 200
Learning rate warmup epochs	2, 3, 4
Learning rate warmup factor	0.2
Max # of Epochs	300, 500, 1000, 2000